The Structural Properties of Major White Matter Tracts in Strabismic Amblyopia

Yiran Duan,[1] Anthony M. Norcia,[1] Jason D. Yeatman,[2] and Aviv Mezer[3]

[1]Department of Psychology, Stanford University, Stanford, California, United States
[2]Institute for Learning and Brain Science (ILABS), University of Washington, Seattle, Washington, United States
[3]Edmond & Lily Safra Center for Brain Sciences, The Hebrew University of Jerusalem, Jerusalem, Israel

Correspondence: Yiran Duan, Department of Psychology, Stanford University, Stanford, CA 94305, USA; yirand@gmail.com.

Submitted: April 14, 2015
Accepted: June 15, 2015

Citation: Duan Y, Norcia AM, Yeatman JD, Mezer A. The structural properties of major white matter tracts in strabismic amblyopia. *Invest Ophthalmol Vis Sci*. 2015;56:5152–5160. DOI:10.1167/iovs.15-17097

Purpose. In order to better understand whether white matter structural deficits are present in strabismic amblyopia, we performed a survey of the tissue properties of 28 major white matter tracts using diffusion and quantitative magnetic resonance imaging approaches.

Methods. We used diffusion-based tensor modeling and a new quantitative T1 protocol to measure fractional anisotropy (FA), mean diffusivity (MD), and myelin-sensitive T1 values. We surveyed tracts in the occipital lobe, including the vertical occipital fasciculus (VOF)—a newly rediscovered tract that bridges dorsal and ventral areas of the occipital lobe, as well as tracts across the rest of the brain.

Results. Adults with long-standing strabismic amblyopia show tract-specific elevations in MD. We rank-ordered the tracts on the basis of their MD effect-size. The four most affected tracts were the anterior frontal corpus callosum (ACC), the right VOF, the left inferior longitudinal fasciculus (ILF) and the left optic radiation.

Conclusions. The results suggest that most white matter tissue properties are relatively robust to the early visual insult caused by strabismus. However, strabismic amblyopia does affect MD, not only in occipital tracts, such as the VOF and optic radiation, but also in long range association tracts connecting visual cortex to the frontal and temporal lobes (ILF) and connecting the two hemispheres (ACC).

Keywords: strabismus, amblyopia, white matter, tractography, diffusion-MRI

Amblyopia is a developmental disorder that is characterized by unilateral (or less commonly, bilateral) reduction of best-corrected visual acuity that cannot be directly attributed to pathology of the eye. Understanding the neural basis of amblyopia is important both for clinical applications and for understanding the association of early visual experience and brain plasticity.[1,2]

Functional neuroimaging has revealed changes in patterns of brain activation in patients with amblyopia compared with control subjects.[3] Early in the visual pathway, the lateral geniculate nucleus (LGN) shows reduced activation when driven by the amblyopic compared with the fellow eye.[4,5] Downstream from the LGN, reduced activation has also been found in the primary visual cortex (V1),[6–9] as well as in high-order cortical areas involved in face perception,[10] multiobject tracking,[11] and visual-guided actions.[12]

In addition to changes in neural responses, structural neuroimaging has helped us understand the biological underpinnings of the behavioral differences in terms of changes in the structure of either grey matter[13–19] or white matter.[19–23] Grey matter contains cell bodies and is where neural computations take place. Structural changes in grey matter have been quantified via voxel-based morphometry (VBM), a technique that quantifies differences in brain shape between patients and controls.[24] Studies using VBM have detected grey matter changes mainly in the bilateral calcarine sulcus[13–16]; but changes in extrastriate areas such as the parietal-occipital junction, ventral temporal cortex, superior and inferior frontal gyrus[13–15] have also been reported.

White matter is composed of bundles of axons that transmit signals between various cortical or subcortical areas. Analyses of white matter changes can provide additional insight into the pathophysiology of amblyopia because the function of a given brain area depends not only on the activity of neuronal populations within that area, but also on the interactions mediated by white matter connections between this brain area and other areas.[25] The integrity of the white matter can be studied through examining volume changes or specific tissue property changes. To study white matter volume changes, researchers have applied VBM to voxels that are classified as white matter and have found decreased volume in the white matter around the primary visual cortex, right premotor cortex, bilateral dorsolateral prefrontal cortex, bilateral cingulate cortex, and the bilateral optic radiations.[19,22,23] By contrast, increases in white matter volume have been reported in the bilateral cuneus areas and the right inferior frontal gyrus.[23]

Diffusion tensor imaging, on the other hand, probes tissue properties at the micrometer scale within a magnetic resonance imaging (MRI) voxel by modeling movement of water molecules in multiple directions. In white matter, where myelinated axons are directionally coherent, water molecules diffuse much more easily along the length of the axons than perpendicular to them. Thus, the rate of water diffusion is greatest in the direction parallel to the principal orientation of an axon bundle and is reduced in all directions perpendicular

to the principal direction.[26] Because axon orientation affects the diffusion process, the trajectory of white matter fibers can be reconstructed by tracing the principal diffusion direction from one voxel to a neighboring voxel.[27] Hence, based on diffusion measurements, specific white matter connections can be traced within an individual's brain and measures of diffusion properties within these connections can be used to gain insight into organization of the fiber tract.

Voxel-based analyses of diffusion images have revealed various changes in white matter properties in amblyopia patients. For example, studies of children with anisometropic amblyopia found changes both in the rate of water diffusion and in the coherence of diffusion directions in various regions of interest, but the findings were not highly consistent.[23,28,29] More specifically, four studies have selectively examined the optic radiation using fiber tractography, but the results have also been mixed.[20,21,30,31]

The diversity of structural imaging results may reflect the diversity inherent in the disorder. First, there are three main subtypes of amblyopia: strabismic, anisometropic, and form deprivation.[32] The mixed findings are possibly due to the fact that different types of amblyopia may have distinct impacts on specific brain structures. Moreover, prior studies have either used small sample sizes ($n < 10$) or samples with mixed etiologies. Each study has used a slightly different set of scanning and tracking parameters. For example, over the available studies of white matter, the image voxel size ranges from 4 to 1.6 mm^3, and the number of diffusion directions measured ranges from 13 to 32 (more directions give better tractography results). Finally, fractional anisotropy (FA) and mean diffusivity (MD) values reflect a range of geometric and microstructural factors rather than any specific biological properties.[33–35]

With these limitations in mind, the current study focused on one specific subtype of amblyopia—strabismic amblyopia, whose white matter properties have not been systematically studied before, and we used higher resolution measures than previous studies: we reconstructed tracts from 96-direction diffusion images at a voxel size of 2 mm^3. Strabismus is of particular interest because it commonly results in a loss of binocularity as well as a unilateral loss of visual acuity. Functionally, patients with strabismus tend to have a different behavioral phenotype than patients with anisometropia.[36] In addition, rather than focusing on a small number of tracts in the occipital lobe, we made a comprehensive survey of 28 major white matter fiber tracts. The tractography method provides us the opportunity to understand cortical and subcortical connectivity for specific fiber tracts in vivo.[27] Furthermore, in order to resolve the ambiguities from measuring diffusion properties alone, we also employed a new quantitative MRI (qMRI) protocol to map scanner-bias-independent T1 values along each tract. It has been shown that this bias-free T1 value is particularly sensitive to myelin in human white matter.[37]

More specifically, we have three hypotheses in mind. First, as suggested by previous studies,[20,21,30,31] alterations in white matter may take place in the optic radiation that connects the LGN to V1. Secondly, the corpus callosum is of particular interest due to its involvement in binocular integration at the midline. The posterior part of the callosum contains fibers connecting cortical areas representing midline body regions and it plays a major role in binding together the separate representations of the two hemifields at the vertical meridian. Animal studies have found that abnormal binocular experience induced by strabismus affects callosal myelination and the projection areas of callosal fibers, resulting in an inability to unify separate representations of visual fields.[38–41] It is possible that the occipital portion of the corpus callosum is also affected in human strabismic amblyopia. Finally, we have studied a recently rediscovered tract: the vertical-occipital fasciculus (VOF).[42,43] The vertical-occipital fasciculus is the only major fiber bundle known to connect dorsal and ventral regions of occipital, parietal, and temporal cortex. This tract is of interest as it is the only currently known vertical, long-range fiber tract in the occipital lobe and because there is evidence showing that the effects of amblyopia may involve both dorsal and ventral cortical areas that are connected by the VOF.[44,45]

Methods

Participants

Patients. Sixteen adults with strabismic amblyopia (average age = 45.31, SD = 13.26, eight males) participated in the study. Table 1 summarizes their acuity, refractive errors, and stereopsis. All patients had strabismic amblyopia with unmeasurable stereopsis on the Titmus or RandDot stereo tests. They were recruited by advertisements in local print media or electronic data record searches (Stanford Translational Research Integrated Database Environment).

Controls. Each patient was matched with two typically developing controls that were of similar age (±3 years). The 32 age-matched controls (mean age = 45.03, SD = 13.79, 15 males) were recruited from the San Francisco Bay Area and were screened for neurological, psychiatric, and cognitive disorders. They were confirmed to have no structural brain disease and were neurologically healthy. These participants were part of a larger cohort that has been studied previously.[46]

All participants provided informed consent and authorization to use their clinical data for research. The Stanford University Institutional Review Board approved all procedures for medical research involving human subjects.

MRI Acquisition and Processing

All imaging data were collected on MRI equipment (3T General Electric Discovery 750; GE Healthcare, Buckinghamshire, UK) equipped with a 32-channel head coil at the Center for Cognitive and Neurobiological Imaging at Stanford University.

Diffusion-weighted imaging (DWI) data were acquired using dual-spin echo diffusion-weighted sequences with full brain coverage. Diffusion weighting gradients were applied at 96 noncollinear directions across the surface of a sphere as determined by the electrostatic repulsion algorithm.[47] In all subjects, DWI data were acquired at 2.0 mm^3 spatial resolution and diffusion gradient strength was set to $b = 2000$ s/mm^2. The diffusion-weighted imaging data was motion corrected by a rigid body alignment algorithm. A robust fitting method was used for tensor fitting.[48] Preprocessing was implemented in a computing environment (MATLAB; Math Works, Natick, MA, USA) and the analysis tools are publically available as part of the Vistasoft software distribution (https://github.com/vistalab/vistasoft/tree/master/mrDiffusion/dtiInit).

The quantitative T1 parameter was measured from spoiled GE images acquired with different flip angles ($\alpha = 4°$, 10°, 20°, and 30°; repetition time [TR] = 20 ms; echo time [TE] = 2.4 ms). The scan resolutions were 1 mm^3. For calibration of T1, additional spin-echo-recovery (SEIR) scans with echo-planar imaging (EPI) readout (SEIR-epi) were collected. We conducted the SEIR-epi was with a slab inversion pulse and spectral spatial fat suppression. The repetition time was 3 s; echo time was set to minimum full; inversion times were 50, 400, 1200, and 2400 ms. We used a 2-mm^2 in-plane resolution with a slice thickness of 4 mm. The EPI readout was performed using ×2 acceleration to minimize spatial distortions. The image-analyzing pipeline

Investigative Ophthalmology & Visual Science

TABLE 1. Clinical Characteristics of Individuals With Amblyopia

				Visual Acuity			Refractive Error		
No.	Sex	Age	Type	OD	OS	Stereopsis, arcsec	OD	OS	Age of Diagnosis and Surgery
1	F	34	Eso	20/20	20/>400	>400″	$-1.25 = -0.75 \times 169^{\circ}$	$8.25 = -2.00 \times 147^{\circ}$	Diagnosed at 2, surgery at 2
2	F	60	Eso	20/16 + 2	20/63 + 1	>400″	$+2.00 = -0.50 \times 94^{\circ}$	$+4.00 = -0.5 \times 107^{\circ}$	Diagnosed at 8, surgery at 9
3	M	33	Eso	20/80	20/20	>400″	$-2.00 = -1.25 \times 160^{\circ}$	$-1.5 = -1.25 \times 30^{\circ}$	Diagnosed at 4 months, surgery at 1 and 25
4	F	57	Eso	20/25	20/>400	>400″	$-0.5 = -0.5 \times 180^{\circ}$	$-1.75 = -0.75 \times 139^{\circ}$	Diagnosed at 2, no surgery
5	F	44	Eso	20/16	20/63 − 2	>400″	Plano	Plano	Diagnosed at 4, no surgery
6	M	54	Eso	20/20	20/40 − 2	>400″	−6.00	−6.00	Diagnosed at 4, surgery at 4
7	F	43	Eso	20/50 + 2	20/20	>400″	−0.50	$-5.75 = -0.75 \times 70^{\circ}$	Diagnosed at birth, surgery at 1 and 12
8	M	46	Exo	20/125 − 1	20/20 + 1	>400″	$0.50 = +0.75 \times 130^{\circ}$	plano $= -0.75 \times 130^{\circ}$	Diagnosed at birth, surgery at 7
9	M	20	Eso	20/20	20/50	>400″	+2.50	+5.00	Diagnosed at birth, surgery <1
10	F	63	Exo	20/25	20/50 − 1	>400″	−10.25	$-8.76 = -0.75 \times 125^{\circ}$	Diagnosed at birth, no surgery
11	F	33	Eso	20/16 − 1	20/300	>400″	$-0.75 = -0.50 \times 140^{\circ}$	$+6.00 = -1.75 \times 180^{\circ}$	Diagnosed at 3, surgery at 22
12	M	67	Exo	20/125 − 2	20/16 − 1	>400″	+4.00	$+4.25 = +1.25 \times 55^{\circ}$	Diagnosed <4, surgery at 4
13	F	37	Eso	20/100	20/20	>400″	$+2.00 = +1.00 \times 70^{\circ}$	$+3.00 = +1.00 \times 135^{\circ}$	Diagnosed at birth, surgery at 1
14	M	29	Eso	20/20	20/50	>400″	$-1.00 = -0.50 \times 95^{\circ}$	$+0.50 = -1.00 \times 84^{\circ}$	Diagnosed at birth, surgery <1
15	M	59	Eso	20/20 + 1	20/100	>400″	$-1.00 = -1.50 \times 10^{\circ}$	$+0.50 = -1.00 \times 5^{\circ}$	Diagnosed at 3, no surgery
16	M	46	Eso	20/80 − 1	20/12.5	>400″	$-7.50 = -1.00 \times 90^{\circ}$	$-4/25 = -1.75 \times 70^{\circ}$	Diagnosed at 1, no surgery

Eso, esotropia; Exo, exotropia.

can be found as open-source MATLAB code (https://github.com/vistalab/mrQ). This pipeline provided us with a quantitative T1 map for each subject. For a detailed explanation of the analysis procedures and algorithms, see Mezer et al.[33]

White Matter Tract Identification

The automated fiber quantification (AFQ) software package[49] was used to identify 24 fiber tracts using a deterministic streamline tracking algorithm.[27] The corpus callosum was segmented into eight callosal fiber groups by placing two ROIs in homologous regions of each hemisphere. Fractional anisotropy and MD are the most widely used summary indices in diffusion tensor imaging–based brain research. Fractional anisotropy is a scalar ranging from 0 to 1 that quantifies the coherence of water diffusion, with 0 indicating low coherence and 1 indicating high coherence, while MD measured the average rate of water diffusion, with higher rates indicating fewer boundaries for water diffusion; T1 is a myelin-sensitive measurement obtained from qMRI. Each tract was summarized by a vector of 100 values representing the T1, FA, or MD properties sampled at equidistant locations along the tract, and we label this vector as the "tract profile." Figure 1 shows a visualization of this concept. Please see Yeatman et al.[46,49] for a detailed description of the methodology and algorithms used by AFQ (https://github.com/jyeatman/AFQ).

The procedure used to define the VOF is described in detail in Yeatman and Weiner's recent paper.[42] The first step is to generate a whole-brain connectome by probabilistic tractography. Probabilistic tractography assumes a distribution of principal direction of orientations instead of a single orientation, thus it performs better at locations where complicated fiber crossings are present.[50] In order to define the endpoints of the tract, we identified the ventral occipital temporal cortex, including the fusiform, inferior occipital, and inferior temporal gyri from a segmentation of a T1-weighted image using FreeSurfer[51] (http://surfer.nmr.mgh.harvard.edu). Automated fiber quantification was then used to perform fiber tract segmentation and tissue property mapping. These algorithms are distributed as "VOF" toolbox within the AFQ software package (https://github.com/jyeatman/AFQ/tree/master/vof).

The optic radiation was identified by first setting regions of interest in V1 and the LGN. The location of V1 was obtained from an atlas-labeled FreeSurfer segmentation and the location of LGN was defined manually based on the high-resolution anatomical image.[52] We identified the optic radiation as the most likely pathway connecting LGN and V1 using probabilistic tractography based on ConTrack[53] (https://github.com/vistalab/contrack). The tissue property mapping was performed by the AFQ software. A detailed description of this procedure is available.[54]

Data Analysis

To obtain a summary of the tract profile data, we averaged the middle 80 values of each tract profile to obtain a tract mean. We excluded the first and the last 10 points in order to only include unambiguous white matter and not voxels at the gray/white matter interface.[54] We then averaged the tract means over all participants within each group and calculated the signed differences between patients and controls for each tract. We focused on effect size to describe the differences between the groups. The effect size was calculated as $d = \frac{\bar{x}_1 - \bar{x}_2}{s}$ where x is the sample mean and s is the pooled standard deviation.[55] In cases where the effect was large, we also

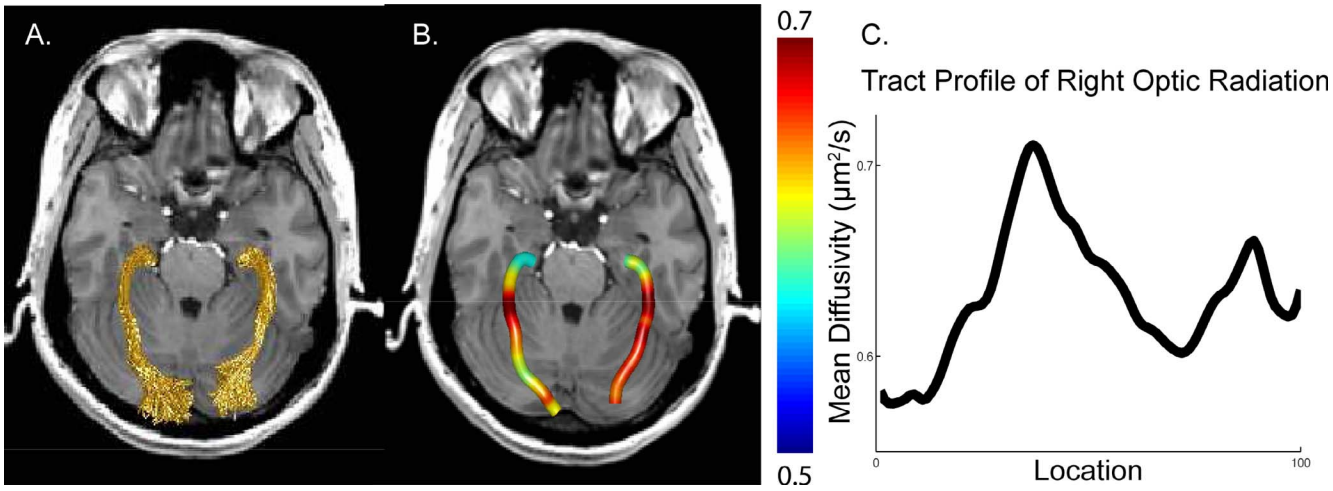

FIGURE 1. Tract profiles. (**A**) Optic radiation identified in a representative subject. (**B**) Values of MD along optic radiation (*red*: high MD; *blue*: low MD). Values of MD were obtained along the tract based on the linear sum of individual voxel MD value weighted by its Mahalanobis distance from the core fiber. (**C**) Value of MD plotted along the optic radiation.

described the common *P* values. Effect size (see below) was used to provide a ranking of the fibers.

We used the R statistical software and lme4[56] package to perform a linear mixed effects analysis on the optic radiation, VOF, and the occipital callosum in order to compare their tract profiles between patients and controls. We entered "subject group" as a fixed effect. As random effects, we had intercept for subjects, as well as by-subject and by-node random slopes for the effect of group. Values of *P* were obtained by likelihood ratio tests of the full model with the effect in question against the model without the effect in question. For the tracts that showed an effect of group, we applied post hoc tests to determine the approximate location of the abnormalities. In order to reduce the dimensionality of the data for this comparison, we averaged the measurements from every 20 nodes, resulting in four summary measurements along each tract.

Finally, in order to determine whether an effect in one tract was due to an effect in a nearby tract, we conducted a distance analysis in relevant tracts. This analysis aimed to check whether effects (if any) along the nodes of one tract were located nearby in space to nodes showing significant differences in the other tract. We identified nodes with significant differences by two-sample *t*-tests. This statistically liberal approach to detecting affected nodes was designed to maximize our ability to capture any possible uncertainties when trying to assign effects uniquely to any one tract. A node-by-node Euclidean distance between pairs of tracts was calculated in the AC-PC standard space, resulting in a distance matrix with the nodes of one tract represented by the horizontal axis and those of the other by the vertical axis.

RESULTS

Macroscopically, there was no tract volume difference between patients and controls and there was no difference between the volume of the ventricles. The percentage differences between patients and controls for the FA and T1 measurements were small across the individual tracts, and most of these differences were not significant. The effect size for mean differences averaged across all the tracts was –0.18 for FA, 0.41 for MD, and 0.20 for T1. We subsequently analyzed the tract profiles for MD because it showed the greatest effect size in tract mean differences.

Tract profiles for the optic radiation, VOF, and occipital corpus callosum were compared between patients and controls. Figure 2 displays a visualization of the optic radiation and the VOF and their tract profile comparisons. The likelihood ratio tests between the full model with mixed effects and the null model revealed significant main effects of group for several tracts. The patients' MD along the left optic radiation was significantly higher than that of the controls ($\chi^2 = 1$, $P = 0.03$). Their mean diffusivity for the right optic radiation was marginally higher than that of the controls ($\chi^2 = 1$, $P = 0.07$). Post hoc tests on dimension-reduced data revealed the approximate locations of abnormality. There were marginally significant group differences at locations close to LGN in both tracts ($P = 0.05$, 0.07, respectively). The tract profile of the right VOF showed significantly higher values in patients ($\chi^2 = 1$, $P = 0.02$) , with a major part of the tract showing a main effect of group (three out of four locations, $P = 0.04$, 0.02, 0.03, respectively) . These locations are indicated by filled red circles in Figure 2. There was no difference between patients and controls in the left VOF or in the occipital callosum (see Supplementary Fig. S1 for a visualization of the occipital callosum).

From the visualizations of the VOF and the optic radiation in Figure 2, it is sometimes difficult to tell if parts of the two tracts are overlapping (i.e., pass through the same voxels). Figure 3 displays the results of the distance analysis for these tracts. The dotted line indicates the possible affected portions in each tract, and the box with a thick border highlights the distance between the affected portions of the two tracts. The color scale plots the Euclidean distance within these affected regions. In regions where the internode distance is small, it is not possible to uniquely assign the effect to one tract or the other. By contrast, when the distance is large (~15 mm) the tracts are sufficiently separated to independently interpret the effect. In Figure 3 left there are effects in the left optic radiation (dashed lines), but no effect in the left VOF. The effect observed in left optic radiation is therefore not due to the effects in the left VOF. In Figure 3 right, both tracts have effects, but the distance between affected portions of the two tracts is more than 20 mms and there are thus independent effects in both tracts.

Turning now to the whole-brain tract analysis, Table 2 provides a ranking of all of the measured fibers by their effect

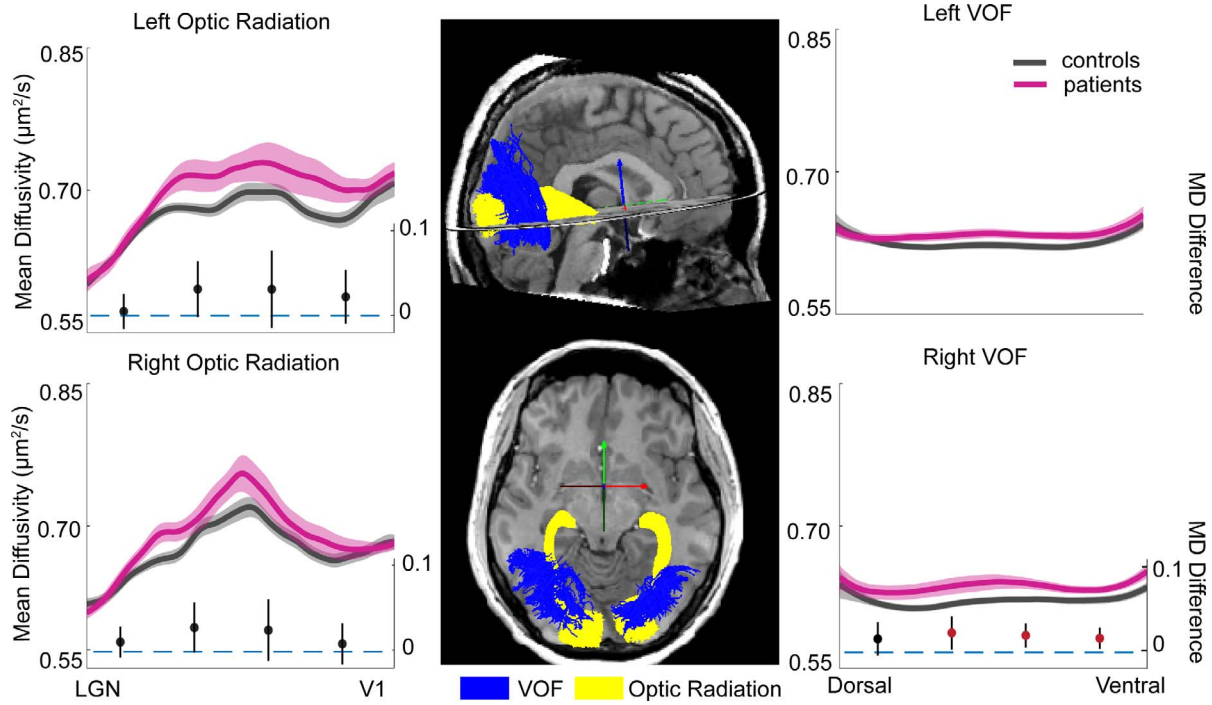

Figure 2. Mean diffusivity along the optic radiation and vertical-occipital fasciculus. The rendering in the *middle panel* shows a visualization of the optic radiation and the VOF in sagittal and axial views. The *left* and the *right* panels show MD in the optic radiation and the VOF. *Thick curves* show the mean of each group (*red*: patient; *black*: control). The *lighter shaded areas* show the range of ±1 SE from the mean. *x-axis* describes normalized position along the tract. The *filled circles* show the differences of the mean (averaged across every 20 nodes) between patients and controls. The lines indicate the 95% confidence intervals of the differences. Significant differences ($P < 0.05$) are marked by *red*.

sizes on the MD tract mean measure. The most affected tract in terms of effect size was the anterior frontal corpus callosum (ACC: $d = 0.74$). Figure 4 shows the tract profiles for the ACC and another top-ranking tract, the left inferior longitudinal fasciculus (ILF). The anterior frontal corpus callosum connects the homologous regions of the anterior frontal lobe in each hemisphere. The inferior longitudinal fasciculus connects the temporal lobe and occipital lobe. Post hoc tests revealed several locations of significant group differences ($P < 0.05$), which are indicated by red circles in Figure 4. Beyond these tracts, there is a graded continuum of effect sizes in the remainder of the tracts analyzed.

As the ILF also lies in the occipital lobe and passes near the optic radiation and the VOF, we performed our distance analysis as above in order to determine if the effects observed in one tract are independent of effects in the other tracts. Figure 5 displays the results of the distance analysis for these tracts. In the left ILF, there are two regions of the tract that show significant effects. Neither of these effects can be accounted for by the left VOF (Fig. 5A) as there are no effects

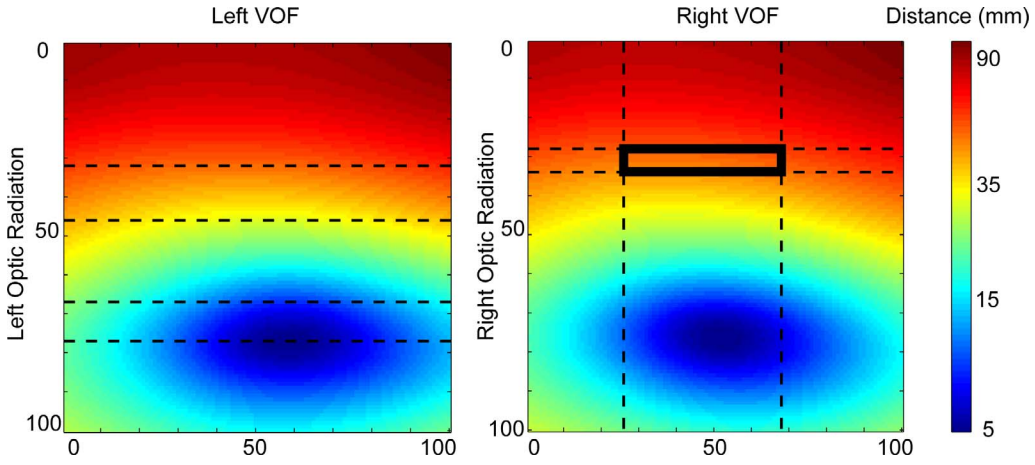

Figure 3. Node-wise distance between optic radiation and vertical-occipital fasciculus. *x-axis* describes normalized position along the VOF; *y-axis* describes normalized position along the optic radiation. The colormap represents the log value of the node-wise Euclidean distance, $\log(\sqrt{x^2 + y^2 + z^2})$, in the standard AC-PC space, with smaller distance represented by *blue* and larger distance represented by *red*. The *dotted line* indicates the affected portion in each tract, and the box in *thick border* highlights the distance between the affected portions of the two tracts. The colorbar scale on the *right* indicates distances converted from log millimeters to millimeters.

Table 2. Fiber Tract Ranking by Effect Size in MD Tract Mean Difference

Ranking	Fiber Tract	*P* Value	Effect Size
1	ACC	0.019	0.74
2	Right VOF	0.023	0.72
3	Left ILF	0.025	0.71
4	Left optic radiation	0.039	0.65
5	Temporal CC	0.063	0.58
6	Superior frontal CC	0.075	0.56
7	Right optic radiation	0.082	0.54
8	Right IFOF	0.097	0.52
9	Left IFOF	0.097	0.52
10	Left arcuate	0.099	0.52
11	Left VOF	0.124	0.48
12	Right SLF	0.126	0.48
13	Right ILF	0.139	0.46
14	Orbital frontal CC	0.141	0.46
15	Right thalamic radiation	0.189	0.41
16	Right arcuate	0.200	0.40
17	Superior parietal CC	0.209	0.39
18	Posterior parietal CC	0.223	0.38
19	Left thalamic radiation	0.242	0.36
20	Left cingulum cingulate	0.264	0.35
21	Left SLF	0.292	0.33
22	Motor CC	0.344	0.29
23	Left uncinate	0.399	0.26
24	Right uncinate	0.521	0.20
25	Left corticospinal	0.644	0.14
26	Occipital CC	0.811	0.07
27	Right corticospinal	0.903	0.04
28	Right cingulum cingulate	0.925	0.03

CC, corpus callosum; IFOF, inferior-longitudinal-occipital fasciculus; SLF, superior-longitudinal fasciculus.

in the left VOF. When considering the relationship of the left ILF to the left optic radiation, there is a single region where the two tracts are too close together to suggest independent effects (upper left box), but there are three other regions that are sufficiently separate to indicate independent effects. In the right occipital lobe, the distance in the potential overlap region between the VOF and the ILF is large but this same region is highly overlapped with the optic radiation. Together with our previous distance analysis, we can conclude the effect in the right VOF is independent of the other two tracts but the effects in the right optic radiation is contaminated with the effects in the right ILF.

Discussion

Adults with long-standing strabismic amblyopia show tract-specific elevations in MD. Elevated MD values may be associated with decreased axonal density or decreased fluid viscosity.[57] The absence of a difference in T1 indicates that demyelination or other change in nonwater tissue volume may not be the predominant deficits in strabismic amblyopia. Different biological sources may affect MD by changing the free space between membranes that hindered the diffusion without dramatically changing the total membrane fractions such as fiber volume fraction[58] and astrocyte organization.[59] The lack of tract-specific effects in FA is possibly due to the fact that FA is much more variable than MD and it can reflect a mixture of several different types of change.[60]

Participants with strabismic amblyopia showed larger MD values (greater diffusivity) in the optic radiation, but no effect in the splenial callosum, replicating a recent study using broadly similar methods.[20] We also provide here the first analysis of the VOF in amblyopia. The vertical occipital fasciculus is the only currently known vertical, long-range white matter tract in the occipital lobe. It connects dorsolateral and ventrolateral visual cortex.[42,43] Dorsal extra-striate visual areas are specialized for analyzing spatial aspects of object features and processing motion-related information, while ventral regions of the occipital and temporal lobes are specialized for form perception and object recognition.[61,62] Our findings suggest that the communication between the two streams may be affected in strabismic amblyopia. This may be one of the reasons that motion defined form is even disrupted in the fellow eye in amblyopia patients.[63] Patients with amblyopia are known to have deficits in visual motion processing[64–66] and in object recognition,[10] and it would be interesting to determine if perceptual integration of form and motion information is particularly disrupted.

Second, from the survey of the rest of the white matter tracts, ACC and left ILF showed significantly higher MD values in patients with strabismic amblyopia. The anterior frontal corpus callosum connects homologous regions of the prefrontal cortex. This brain region is well known for its role in high-level functions such as decision making, executive and impulse control. The abnormality in ACC may contribute to previously reported impairments in visual decision making among adults with amblyopia.[67]

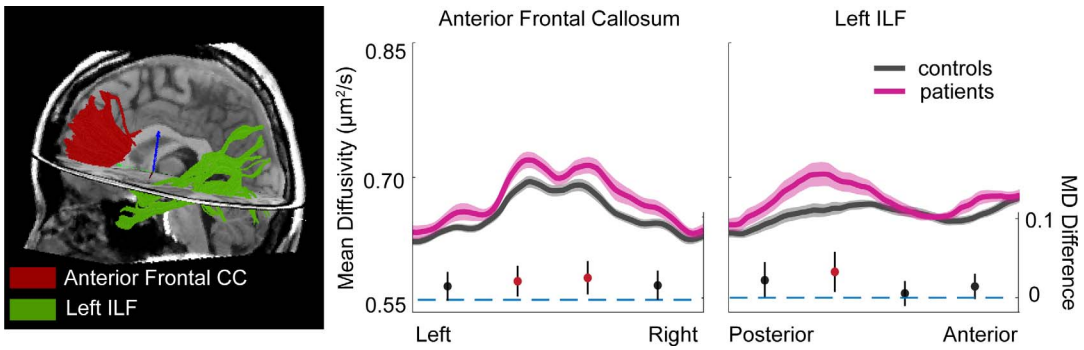

Figure 4. Mean diffusivity along the ACC and the left ILF. The left panel shows a visualization of the fiber tracts. The *middle* and the *right* panels show MD measures along ACC and the left ILF. *Thick curves* show the mean of each group (*red*: patient; *black*: control). The *lighter shaded areas* show range of ±1 SE from the mean. *x-axis* describes normalized position along the tract. The *filled circles* show the differences of the mean (averaged across every 20 nodes) between patients and controls. The *lines* indicate the 95% confidence intervals of the differences. Significant differences ($P < 0.05$) are marked by *red*.

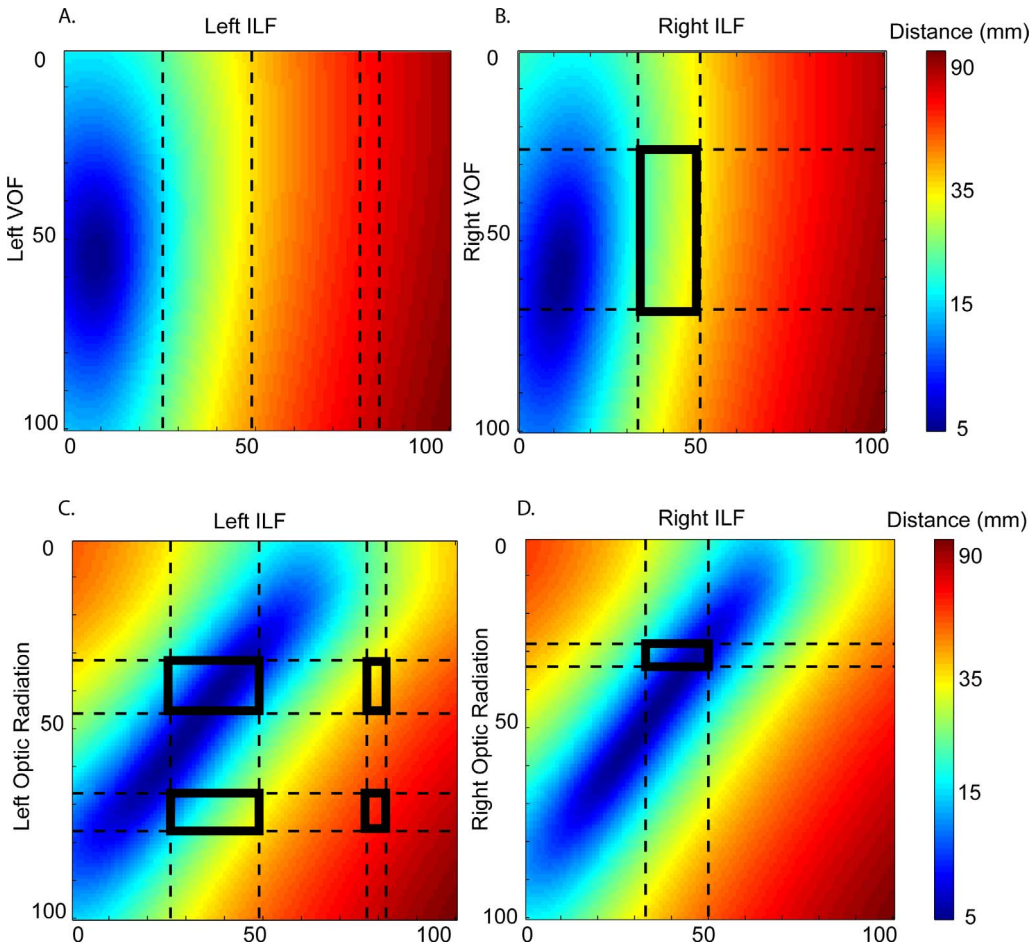

Figure 5. Node-wise distance between inferior longitudinal fasciculus and vertical-occipital fasciculus (**A**, **B**), inferior longitudinal fasciculus and optic radiation (**C**, **D**). *x*- and *y*-*axes* describe normalized positions along the tract. The colormap represents the log value of the node-wise Euclidean distance—$\log(\sqrt{x^2+y^2+z^2})$—in the standard AC-PC space, with smaller distance represented by *blue* and larger distance represented by *red*. The *dotted line* indicates the affected portion in each tract, and the box in thick border highlights the distance between the affected portions of the two tracts. The colorbar scale on the *right* indicates distances converted from log millimeters to millimeters.

The inferior longitudinal fasciculus is a long association fiber bundle interconnecting the occipital lobe and temporal lobe, and it is a major pathway transmitting information between those two areas that are crucial for visual perception and object recognition.[68,69] Abnormalities in the ILF may be associated with behavioral deficits in object recognition among amblyopia patients. However, it was noted very early on that the fibers of the optic radiation intermingle with those of the ILF.[70] Diffusion tensor imaging is limited in its ability to separate tracks that cross or run closely in parallel and thus the effect in ILF could, in principle, also stem from an impairment in the optic radiation, or vice versa. Our distance analysis indeed shows regions of both tracts that are affected and that are very close together. However, we also see independent effects in both tracts in portions that are sufficiently distant to be easily resolved with our methods (see Fig. 5C). To fully understand the functional role of the ILF in vision, it will be important for future work to determine which regions of visual cortex send or receive axons that comprise the ILF.

The present survey of major white matter tracts suggests that most white matter tissue properties are relatively robust to the early visual insult caused by strabismus. However, there are detectable increases in mean diffusivity in the optic radiation, right VOF, ACC, and the left ILF. The presence of structural changes in long-range white matter projections both within the occipital lobe (VOF), between the occipital lobe, and the frontal lobe (ILF) and between hemispheres in frontal cortex are novel results of our survey approach. Future research using tasks that depend on the integrity of these long-range projections may shed light on the functional consequences of these structural alterations for patients with strabismic amblyopia.

Acknowledgments

The authors thank Chuan Hou for conducting eye examinations; Shumpei Ogawa for helping with the segmentation of the optic radiation; Hiromasa Takemura for helping with the segmentation of the vertical occipital fasciculus; and Brian Wandell for access to the data for the normal vision participants.

Supported by Grants EY018875 and EY015790 (AMN).

Disclosure: **Y. Duan**, None; **A.M. Norcia**, None; **J.D. Yeatman**, None; **A. Mezer**, None

References

1. Kanonidou E. Amblyopia: a mini review of the literature. *Int Ophthalmol*. 2011;31:249–256.
2. Levi DM. Linking assumptions in amblyopia. *Vis Neurosci*. 2013;277–287.

3. Joly O, Frankó E. Neuroimaging of amblyopia and binocular vision: a review. *Front Integr Neurosci*. 2014;8:62.
4. Miki A, Liu GT, Goldsmith AG, Liu CS, Haselgrove JC. Decreased activation of the lateral geniculate nucleus in a patient with anisometropic amblyopia demonstrated by functional magnetic resonance imaging. *Ophthalmologica*. 2003;217:365–369.
5. Hess RF, Thompson B, Gole G, Mullen KT. Deficient responses from the lateral geniculate nucleus in humans with amblyopia. *Eur J Neurosci*. 2009;29:1064–1070.
6. Barnes GR, Hess RF, Dumoulin SO, Achtman RL, Pike GB. The cortical deficit in humans with strabismic amblyopia. *J Physiol*. 2001;533(1):281–297.
7. Choi MY, Lee KM, Hwang JM, et al. Comparison between anisometropic and strabismic amblyopia using functional magnetic resonance imaging. *Br J Ophthalmol*. 2001;85: 1052–1056.
8. Lee KM, Lee SH, Kim CY, et al. Binocularity and spatial frequency dependence of calcarine activation in two types of amblyopia. *Neurosci Res*. 2001;40:147–153.
9. Goodyear BG, Nicolle DA, Humphrey GK, Menon RS. BOLD fMRI response of early visual areas to perceived contrast in human amblyopia. *J Neurophysiol*. 2000;84:1907–1913.
10. Lerner Y, Pianka P, Azmon B, et al. Area-specific amblyopic effects in human occipitotemporal object representations. *Neuron*. 2003;40:1023–1029.
11. Secen J, Culham J, Ho C, Giaschi D. Neural correlates of the multiple-object tracking deficit in amblyopia. *Vision Res*. 2011;51:2517–2527.
12. Wang T, Li Q, Guo M, et al. Abnormal functional connectivity density in children with anisometropic amblyopia at resting-state. *Brain Res*. 2014;1563:41–51.
13. Chan ST, Tang KW, Lam KC, Chan LK, Mendola JD, Kwong KK. Neuroanatomy of adult strabismus: a voxel-based morphometric analysis of magnetic resonance structural scans. *Neuroimage*. 2004;22:986–994.
14. Mendola JD, Conner IP, Roy A, et al. Voxel-based analysis of MRI detects abnormal visual cortex in children and adults with amblyopia. *Hum Brain Mapp*. 2005;25:222–236.
15. Xiao JX, Xie S, Ye JT, et al. Detection of abnormal visual cortex in children with amblyopia by voxel-based morphometry. *Am J Ophthalmol*. 2007;143:489–493.
16. Lv B, He H, Li X, et al. Structural and functional deficits in human amblyopia. *Neurosci Lett*. 2008;437:5–9.
17. Du H, Xie B, Yu Q, Wang J. Occipital lobe's cortical thinning in ametropic amblyopia. *Magn Reson Imaging*. 2009;27:637–640.
18. Barnes GR, Li X, Thompson B, Singh KD, Dumoulin SO, Hess RF. Decreased gray matter concentration in the lateral geniculate nuclei in human amblyopes. *Invest Ophthalmol Vis Sci*. 2010;51:1432–1438.
19. Liu SY, Zhang J, Zhang Q, et al. A voxel-based-analysis of brain stucture in children with anisometropia. *Chin J Radiol*. 2012; 46(001):45–48.
20. Allen B, Spiegel DP, Thompson B, Pestilli F, Rokers B. Altered white matter in early visual pathways of human amblyopes [published online ahead of print January 20, 2015]. *Vision Res*. doi:10.1016/j.visres.2014.12.021.
21. Xie S, Gong GL, Xiao JX, et al. Underdevelopment of optic radiation in children with amblyopia: a tractography study. *Am J Ophthalmol*. 2007;143:642–646.
22. Jiang Q, Li Q, Guo M, Han W. VBM analysis of white matter volume in children with ametropic amblyopia. *Proc IEEE Biomed Eng Informat*. 2012:387–390.
23. Li Q, Jiang Q, Guo M, Li Q, Cai C, Yin X. Grey and white matter changes in children with monocular amblyopia: voxel-based morphometry and diffusion tensor imaging study. *Br J Ophthalmol*. 2013;97:524–529.
24. Ashburner J, Friston KJ. Voxel-based morphometry—the methods. *Neuroimage*. 2000;11:805–821.
25. Stam C. Use of magnetoencephalography (MEG) to study functional brain networks in neurodegenerative disorders. *J Neurol Sci*. 2010;289:128–134.
26. Le Bihan D. Looking into the functional architecture of the brain with diffusion MRI. *Nature Rev Neurosci*. 2003;4:469–480.
27. Basser PJ, Pajevic S, Pierpaoli C, Duda J, Aldroubi A. In vivo fiber tractography using DT-MRI data. *Magn Reson Med*. 2000; 44:625–632.
28. Wu J, Zeng HW, Fang DG, et al. A study of the optic radiation and corpus callosum by diffusion tensor imaging. *J Clin Ophthalmol*. 2012;20:364–367.
29. Gümüstas S, Altintas O, Anik Y, et al. Anterior visual pathways in amblyopia: quantitative assessment with diffusion tensor imaging. *J Pediatr Ophthalmol Strabismus*. 2012;50:369–374.
30. Song H, Qi S, Tang HH, Yu FJ, Liu LQ. MR DTI and DTT study on the development of optic radiation in patients with anisometropia amblyopia. *Sichuan Da Xue Bao YI Yue Ban*. 2010;41:648–651.
31. Xiao MY, Xu J, Li YJ, Wei X, Peng XJ, He Z. Study on the white matter structure of visual pathway in children with anisometropic amblyopia by diffusion tensor imaging. *Chin Ophthalmol*. 2009:315–320.
32. Barrett BT, Bradley A, McGraw PV. Understanding the neural basis of amblyopia. *Neuroscientist*. 2004;10:106–117.
33. Mezer A, Yeatman JD, Stikov N, et al. Quantifying the local tissue volume and composition in individual brains with magnetic resonance imaging. *Nat Med*. 2013;19:1667–1672.
34. Beaulieu C. The basis of anisotropic water diffusion in the nervous system–a technical review. *NMR Biomed*. 2002;15: 435–455.
35. Paus T. Growth of white matter in the adolescent brain: myelin or axon? *Brain Cogn*. 2010;72:26–35.
36. McKee SP, Levi DM, Movshon JA. The pattern of visual deficits in amblyopia. *J Vis*. 2003;3:380–304.
37. Stueber C, Morawski M, Schafer A, et al. Myelin and iron concentration in the human brain: a quantitative study of MRI contrast. *Neuroimage*. 2014;93:95–106.
38. Innocenti G. Growth and reshaping of axons in the establishment of visual callosal connections. *Science*. 1981; 212:824–827.
39. Innocenti G, Frost D. Effects of visual experience on the maturation of the efferent system to the corpus callosum. *Nature*. 1979;280:231–234.
40. Milleret C, Houzel JC. Visual interhemispheric transfer to areas 17 and 18 in cats with convergent strabismus. *Eur J Neurosci*. 2001;13:137–152.
41. Markham JA, Herting MM, Luszpak AE, Juraska JM, Greenough WT. Myelination of the corpus callosum in male and female rats following complex environment housing during adulthood. *Brain Res*. 2009;1288:9–17.
42. Yeatman JD, Weiner K, Pestilli F, Rokem A, Mezer A, Wandell BA. The vertical occipital fasciculus: A century of controversy resolved by in vivo measurements. *Proc Natl Acad Sci*. 2014; 111:E5214–E5223.
43. Takemura H, Rokem A, Winawer J, Yeatman JD, Wandell BA, Pestilli F. A major human white matter pathway between dorsal and ventral visual cortex [published online ahead of print March 31, 2015]. *Cereb Cortex*. doi:10.1093/cercor/bhv064.
44. Simmers AJ, Ledgeway T, Hess RF. The influences of visibility and anomalous integration processes on the perception of

global spatial form versus motion in human amblyopia. *Vision Res*. 2005;45:449–460.

45. Hamm LM, Black J, Dai S, Thompson B. Global processing in amblyopia: a review. *Front Psychol*. 2014;5:1–21.
46. Yeatman JD, Wandell BA, Mezer A. Lifespan maturation and degeneration of human brain white matter. *Nat Commun*. 2014;5:4932.
47. Jones D, Horsfield M, Simmons A. Optimal strategies for measuring diffusion in anisotropic systems by magnetic resonance imaging. *Magn Reson Med*. 1999;42:515–25.
48. Chang LC, Jones DK, Pierpaoli C. RESTORE: robust estimation of tensors by outlier rejection. *Magn Reson Med*. 2005;53: 1088–1095.
49. Yeatman JD, Dougherty RF, Myall NJ, Wandell BA, Feldman HM. Tract profiles of white matter properties: automating fiber-tract quantification. *PLoS One*. 2012;7:e49790.
50. Descoteaux M, Deriche R, Knosche TR, Anwander A. Deterministic and probabilistic tractography based on complex fibre orientation distributions. *IEEE Trans Med Imaging*. 2009;28:269–286.
51. Fischl B. FreeSurfer. *Neuroimage*. 2012;62:774–781.
52. Horton JC, Landau K, Maeder P, Hoyt WF. Magnetic resonance imaging of the human lateral geniculate body. *Arch Neurol*. 1990;47:1201–1206.
53. Sherbondy AJ, Dougherty RF, Ben-Schachar M, Napel S, Wandel BA. ConTrack: finding the most likely pathways between brain regions using diffusion tractography. *J Vis*. 2008;8(9):1–16.
54. Ogawa S, Takemura H, Horiguchi H, et al. White matter consequences of retinal receptor and ganglion cell damage. *Invest Ophthalmol Vis Sci*. 2014;55:6976–6986.
55. Ferguson CJ. An effect size primer: a guide for clinicians and researchers. *Prof Psychol Res Pr*. 2009;40:532.
56. Bates D, Maechler M, Bolker B. lme4: linear mixed-effects models using S4 classes. Available at http://cran.stat.ucla.edu/web/packages/lme4/. Accessed May 29, 2015.
57. Alexander AL, Lee JE, Lazar M, Field A. Diffusion tensor imaging of the brain. *Neurotherapeutics*. 2007;4:316–329.
58. Stikov N, Perry LM, Mezer A, et al. Bound pool fractions complement diffusion measures to describe white matter micro and macrostructure. *Neuroimage*. 2011;54:1112–1121.
59. Blumenfeld-Katzir T, Pasternak O, Dagan M, Assaf Y. Diffusion MRI of structural brain plasticity induced by a learning and memory task. *PLoS One*. 2011;6:e20678.
60. Alexander AL, Hurley SA, Samsonov AA, et al. Characterization of cerebral white matter properties using quantitative magnetic resonance imaging stains. *Brain Connect*. 2011;1: 423–446.
61. Ungerleider LG, Haxby JV. 'What' and 'where' in the human brain. *Curr Opin Neurobiol*. 1994;4:157–165.
62. de Haan EH, Cowey A. On the usefulness of 'what' and 'where' pathways in vision. *Trends Cogn Sci*. 2011;15:460–466.
63. Giaschi DE, Regan D, Kraft SP, Hong XH. Defective processing of motion-defined form in the fellow eye of patients with unilateral amblyopia. *Invest Ophthalmol Vis Sci*. 1992;33: 2483–2489.
64. Simmers A, Ledgeway T, Mansouri B, Hutchinson CV, Hess RF. The extent of the dorsal extra-striate deficit in amblyopia. *Vision Res*. 2006;46:2571–2580.
65. Simmers AJ, Ledgeway T, Hess RF, McGraw PV. Deficits to global motion processing in human amblyopia. *Vision Res*. 2003;43:729–738.
66. Thompson B, Villeneuve MY, Casanova C, Hess RF. Abnormal cortical processing of pattern motion in amblyopia: evidence from fMRI. *Neuroimage*. 2012;60:1307–1315.
67. Farzin F, Norcia AM. Impaired visual decision-making in individuals with amblyopia. *J Vis*. 2011;11:6.
68. Tusa RJ, Ungerleider LG. The inferior longitudinal fasciculus: a reexamination in humans and monkeys. *Ann Neurol*. 1985;18: 583–591.
69. Ortibus E, Verhoeven J, Sunaert S, Casteels I, de Cock P, Lagae L. Integrity of the inferior longitudinal fasciculus and impaired object recognition in children: a diffusion tensor imaging study. *Dev Med Child Neurol*. 2012;54:38–43.
70. Davis LE. An anatomic study of the inferior longitudinal fasciculus. *Arch Neurol Psychiatry*. 1921;5:370–381.